

Review

Strain Accommodations among Twin Variants in Ti and Mg

Ping Zhou^{1,2,*}  and Guo-Zhen Zhu^{2,*} ¹ Institute of Materials, China Academy of Engineering Physics, Jiangyou 621908, China² Department of Mechanical Engineering, University of Manitoba, Winnipeg, MB R3T 5V6, Canada

* Correspondence: ping.zhou@umanitoba.ca or success0066@126.com (P.Z.);

Guozhen.Zhu@umanitoba.ca (G.-Z.Z.)

Abstract: The selection of twin variants has a great influence on deformation texture and mechanical property in hcp metals where slip systems are limited and twinning types are abundant during deformation. Local strain accommodations among twin variants are considered to shed light on variant selection rules in Ti and Mg alloys. Five kinds of strain accommodations are discussed in terms of different regions that are affected by the twinning shear of primary twin. These regions contain (I) the whole sample, (II) neighboring grain, (III) adjacent primary twin in neighboring grain, (IV) adjoining primary twin within the same parent grain, and (V) multi-generation of twinning inside the primary twin. For a potentially active variant, its operation needs not only relatively higher resolved shear stress but also easily accommodated strain by immediate vicinity. Many of the non-Schmid behaviors could be elucidated by local strain accommodations that variants with relatively higher SFs hard to be accommodated are absent, while those with relatively lower SFs but could be easily accommodated are present.

Keywords: strain accommodation; twin variant; titanium; magnesium



Citation: Zhou, P.; Zhu, G.-Z. Strain Accommodations among Twin Variants in Ti and Mg. *Crystals* **2021**, *11*, 453. <https://doi.org/10.3390/cryst11040453>

Academic Editors: Pooya Sareh and Yao Chen

Received: 30 March 2021

Accepted: 17 April 2021

Published: 20 April 2021

Publisher's Note: MDPI stays neutral with regard to jurisdictional claims in published maps and institutional affiliations.



Copyright: © 2021 by the authors. Licensee MDPI, Basel, Switzerland. This article is an open access article distributed under the terms and conditions of the Creative Commons Attribution (CC BY) license (<https://creativecommons.org/licenses/by/4.0/>).

1. Introduction

Unlike cubic metals, hexagonal closed-packed (hcp) metals, such as Ti and Mg, likely have strong contributions of twinning, in addition to that of slip, to their mechanical response. Depending on the c/a ratio of hcp lattice, there are diverse contributions of twinning and slip, leading to different textures and further modifications in mechanical response.

From the viewpoint of stress, deformation modes subjected to the highest or relatively higher resolved shear stress would tend to activate among all the possible modes. The relative quantity of resolved shear stress can be characterized by Schmid factor (SF) $m = \cos\lambda \cdot \cos\mu$, where λ and μ are angles between loading and slip or twinning direction and slip or twinning plane normal, respectively [1]. The m ranges from -0.5 to 0.5 . Generally, deformation modes with SFs greater than 0.3 are considered as active during plastic deformation. By multiplying SF with applied stress corresponding to the initiation of a given deformation mode, the critical resolved shear stress (CRSS) of the specific deformation mode could be determined experimentally. For example, the CRSS for deformation modes in Ti (with a c/a ratio of 1.587) from low to high is $\langle a \rangle$ -type prismatic slip, $\langle a \rangle$ -type basal slip, $\langle c+a \rangle$ -type pyramidal slip and twinning [2,3]. While, in Mg (with a c/a ratio of 1.624), the order is $\langle a \rangle$ -type basal slip, $\{10\bar{1}2\}\langle 10\bar{1}\bar{1} \rangle$ extension twin, prismatic slip, pyramidal slip and $\{10\bar{1}1\}\langle 10\bar{1}2 \rangle$ contraction twin [4–6]. (According to Taylor law, five deformation modes are necessary to satisfy the deformation accommodation condition; twinning is usually involved for plastic deformation).

The abundance of twinning and twin variants makes the selected deformation mode a complex issue. In pure α -titanium (Ti), six types of twinning modes, including three extension twins, $\{10\bar{1}2\}\langle \bar{1}011 \rangle$, $\{11\bar{2}1\}\langle \bar{1}126 \rangle$ and $\{11\bar{2}3\}\langle \bar{1}122 \rangle$, and three contraction twins, $\{1122\}\langle 1123 \rangle$, $\{1124\}\langle 2243 \rangle$ and $\{1011\}\langle 1012 \rangle$, have been observed so far. They generate 36 kinds of primary twin variants as each twin mode has six equivalent variants. If those primary twins undergo further twinning, there are up to 36^2 kinds of possible double-twinning

combinations. In pure magnesium, two twinning modes, $\{10\bar{1}2\}\langle\bar{1}011\rangle$ and $\{10\bar{1}1\}\langle\bar{1}0\bar{1}2\rangle$, induce 12 kinds of primary twins and 12^2 kinds of second-generation twinning.

Two main forms of expressing SFs, including SF curve [7] and SF-inversed pole figure (IPF) [8], are applied to estimate the relative activities of twinning. The latter one, also named as the apparent SF, is more perceptive, because it plots the loading domain for a specific twin variant with all the possible SFs into an IPF, which is associated with a crystallographic coordinate system of parent grain. This method has advantages of calculating the SFs of the multigeneration of twinning [9–11]. The normalized SF, defined as the ratio of each SF to the highest SF, is also adopted in cases that the absolute values of SFs for most twin variants are relatively low due to grain orientation [12,13]. Hence, the normalized SFs range from -1 to 1 . In most cases, the Schmid law has demonstrated success in explaining the twin variant selections [14–18] and deformation texture [19]. However, some non-Schmid behaviors have been observed in Ti [20–22] and Mg [23–28], where the active deformation twins exhibit relatively lower SFs while those with higher or highest SFs are absent.

On the other hand, strain is another key factor determining the operation of various deformation modes, especially in circumstances where the local stress is strongly different from that of the external stress. The accumulated local stress induced by twinning shear needs to relax through plastic strain in the vicinity of twins. The concept of strain accommodation, firstly proposed by Mahajan and Chin [29], characterizes the accommodation abilities of a twinning mode. Later, a quantitative expression of strain accommodation in terms of displacement gradient accommodation (DGA) was reported by Ando et al. [30], Martin et al. [31] and Jonas et al. [32], independently. The DGA calculation and its general form has been extensively used in interactions of twin–twin and twin–slip in both experiment analyses [10,29,33] and theoretical calculations [34].

In this paper, the principle of DGA associated with twinning is elucidated in detail by the aid of the schematic diagram, and the practical applications of DGA criterion are reviewed.

2. Principle of DGA Criterion

Twin is formed by homogeneous shearing of a matrix on the twin plane (or habit plane) along the twin direction; therefore, twin shear can be expressed as a strain tensor of the second rank in the twin coordinate system and transformed linearly. Figure 1a schematically indicates a typical kind of twin behavior inside parent grain A and adjacent grain B. Primary twin p inside grain A adjoins another primary twin n inside a neighboring grain B. Meanwhile, another primary twin variant v inside A interacts with p, which is furtherly twinned into secondary twin s.

To facilitate the expression and extinguish different kinds of coordinate systems, the crystallographic coordinate system is denoted as C , and twin reference system is presented as T . The superscript of coordinate system notation indicates the matrix crystal. Here, the crystallographic coordinate system of grain A (marked by the X , Y and Z axes) are denoted as C^A in Figure 1b, and the crystal frame of twin p is marked as C^p in Figure 1c. It is worth noting that the same twin plane of primary twin p can be expressed either in parent grain frame C^A as a gray plane in Figure 1b or in the crystal framework of the twin C^p as the orange plane in Figure 1c, but they have different indices. The X , Y and Z axes in frame C^p are defined as: $X \parallel \langle\bar{1}2\bar{1}0\rangle$, $Z \parallel [0001]$ and $Y \parallel \langle 10\bar{1}0\rangle$. The twin coordinate system of twin p inside grain A (marked by the x , y and z axes) is denoted as $T^{A \rightarrow p}$, as shown in Figure 1b, while twin frame of twin p inside the twin lattice is represented as T^p . The definition of the twin frame is $x \parallel \eta_1$ (twinning direction), $z \parallel K_1$ normal (K_1 is twin plane), and the y -axis is determined by the cross product of the x and z axes. For a specific twin of type I that has rational indices for K_1 and η_2 , twin frame $T^{A \rightarrow p}$ coincides with twin frame T^p by rotating 180° around the normal plane of K_1 . While, for the type II twin with rational indices for K_2 and η_1 , the two frames overlapped by rotating 180° around the η_1 direction. All the coordinate systems associated with twins in Figure 1a are listed in Table 1.

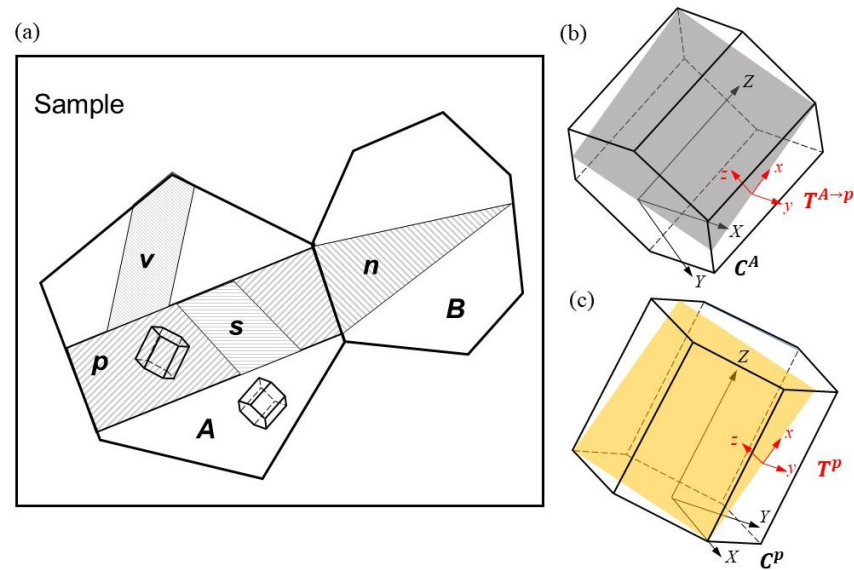


Figure 1. (a) Illustration of twin interactions between grain A and B. Primary twin marked as p in grain A adjacent to the primary twin marked as n in grain B. Another twin variant labeled as v interacts with p within which secondary twin s appears; (b) coordinate systems expressed in the crystal of grain A; (c) coordinate systems expressed in primary twin p.

Table 1. Coordinate systems and corresponding DGT.

Coordinate System Definition	Coordinate System Symbol	DGT in Varied Frames
twin p in crystal frame A	$T^{A \rightarrow p}$	$e_{ij}^{T^{A \rightarrow p}}$
crystal frame of grain A	C^A	$e_{ij}^{C^A}$
Sample reference frame	S	e_{ij}^S
crystal frame of grain B	C^B	$e_{ij}^{C^B}$
twin n in crystal frame B	$T^{B \rightarrow n}$	$e_{ij}^{T^{B \rightarrow n}}$
twin v in crystal frame A	$T^{A \rightarrow v}$	$e_{ij}^{T^{A \rightarrow v}}$
twin frame of primary twin p	T^p	$e_{ij}^{T^p}$
crystal frame of primary twin p	C^p	$e_{ij}^{C^p}$
2nd twin s in crystal frame p	$T^{p \rightarrow s}$	$e_{ij}^{T^{p \rightarrow s}}$

It should be noted that coordinate systems are built over dislocation slip with $x \parallel$ slip direction, $z \parallel$ slip plane normal and y is vertical to the xz plane [26,35], for cases investigating the strain accommodation between the twins and slips. The relationship between the axes of the slip frame and various slip systems for hcp metals are listed in Table 2. Note that slip shear is defined as the magnitude of slip Burgers vector divided by the interplane distance of slip plane for the sake of comparison qualitatively, although dislocation slips do not produce a specific shearing value as twinning.

Table 2. The x , y and z axes of the slip reference frame for different slip systems in hcp metals ¹.

Slip Types	Indices of Slip System	x -axis	y -axis	z -axis
basal $\langle a \rangle$	$(0001) \langle 11\bar{2}0 \rangle$	$\langle 11\bar{2}0 \rangle$	$\langle 10\bar{1}0 \rangle$	$[0001]$
prismatic $\langle a \rangle$	$\{10\bar{1}0\} \langle 11\bar{2}0 \rangle$	$\langle 11\bar{2}0 \rangle$	$[0001]$	$\langle 10\bar{1}0 \rangle$
1st-order pyramidal $\langle a \rangle$	$\{10\bar{1}1\} \langle 11\bar{2}0 \rangle$	$\langle 11\bar{2}0 \rangle$	$\langle 1\bar{1}00 \rangle$	$\langle 11\bar{2} \frac{3}{2r^2} \rangle$
1st-order pyramidal $\langle c+a \rangle$	$\{10\bar{1}1\} \langle 11\bar{2}\bar{3} \rangle$	$\langle 11\bar{2}\bar{3} \rangle$	$\langle 1\bar{1}00 \rangle$	$\langle 11\bar{2} \frac{3}{2r^2} \rangle$
2nd-order pyramidal $\langle c+a \rangle$	$\{11\bar{2}\bar{2}\} \langle 11\bar{2}\bar{3} \rangle$	$\langle 11\bar{2}\bar{3} \rangle$	$\langle 1\bar{1}00 \rangle$	$\langle 11\bar{2} \frac{1}{r^2} \rangle$

¹ r is the c/a ratio of the hcp lattice.

With the above coordinate systems, the displacement gradient tensor (DGT) and its components get physical meaning. Taking displacement along the x , y and z directions as u , v and w , respectively, then the components of DGT could be written as e_{ij} , as shown in Table 3. In the twin reference frame, only the e_{xz} component gets a value of twinning shear s , while the other eight components are zeros. The value s is a constant for a specific twin. The e_{xy} and e_{yx} components correspond to single and double prismatic slips, respectively. The e_{xz} and e_{yz} components correlate to single and double basal slips, respectively. The e_{zx} and e_{zy} components stand for $\langle c+a \rangle$ slips or twinning. All the DGTs expressed in different systems are also listed in Table 1, where the superscript of each e_{ij} corresponds to the coordinate system it is expressed in.

Table 3. Displacement gradient tensor expression.

DGT	DGT in Twin Frame	DGT in Crystallographic Frame
$e_{ij} = \begin{pmatrix} \frac{\partial u}{\partial x} & \frac{\partial u}{\partial y} & \frac{\partial u}{\partial z} \\ \frac{\partial v}{\partial x} & \frac{\partial v}{\partial y} & \frac{\partial v}{\partial z} \\ \frac{\partial w}{\partial x} & \frac{\partial w}{\partial y} & \frac{\partial w}{\partial z} \end{pmatrix}$	$e_{ij}^T = \begin{pmatrix} 0 & 0 & s \\ 0 & 0 & 0 \\ 0 & 0 & 0 \end{pmatrix}$	$e_{ij}^C = \begin{pmatrix} e_{xx} & e_{xy} & e_{xz} \\ e_{yx} & e_{yy} & e_{yz} \\ e_{zx} & e_{zy} & e_{zz} \end{pmatrix}$

There is another definition of a twin coordinate system defined by Ando et al. [30], which is the $y \parallel \eta_1$, $z \parallel K_1$ normal plane and x perpendicular to the yz plane. With such a definition, the initial twinning shear tensor gets a different form shown below:

$$e_{ij} = \begin{pmatrix} 0 & 0 & 0 \\ 0 & 0 & s \\ 0 & s & 0 \end{pmatrix}$$

This kind of definition is different from that of Jonas et al. [32] that is used more extensively, as its twinning shear strain tensor has a much simpler form. Therefore, we adopted the latter, simpler one in the following content.

Based on the coordinate systems defined in Table 1, DGA among different twin variants in Figure 1a can be evaluated through DGT calculation. The flowchart in Figure 2 sorts twin-related DGA evaluations into five categories, numbered from I to V in terms of the aim frames the transformation ended. For each case, twin shear expressed in twin frames could be transformed into other frames to evaluate the strain accommodations that the twin imposed on them. DGTs in black squares are connected by transform matrices with notations shown above the dashed-line arrows. Detailed procedures of the transformation for each category are given in the Appendix A. The application of DGA in these five cases are discussed in Section 3.

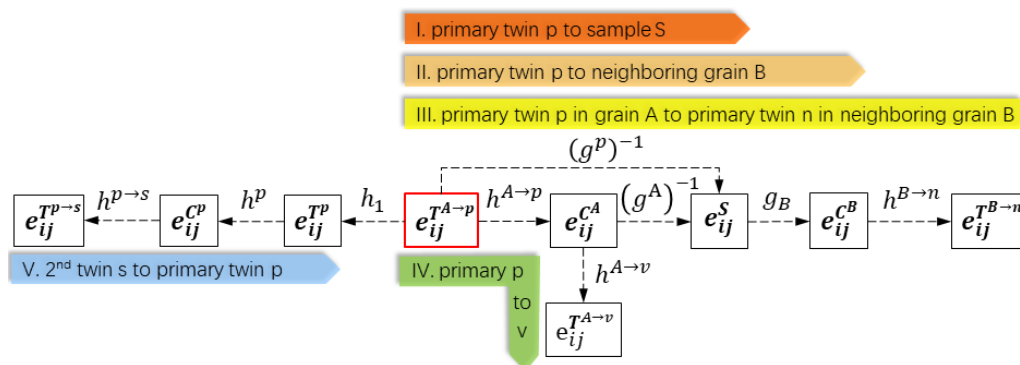


Figure 2. Procedures for calculating twin-related strain accommodation.

3. Application of DGA Criterion

3.1. DGA between Primary Twin and Sample

The contribution of twin shear resulted from primary twin to external strain can be evaluated by transforming DGT $e_{ij}^{T^{A-p}}$ of primary twin p expressed in the crystal frame of grain A into e_{ij}^S expressed in the sample frame, as case I in Figure 2 shows. The aim of the transformation is to evaluate whether the twin shear complies with the external strain or not. Shun et al. [36] investigated strains that $\{11\bar{2}2\}$ - $\{10\bar{1}2\}$ twin pairs appeared at high-angle grain boundaries and contributed to macroscopic loading in rolled pure Ti compressed along the normal direction (ND). The sample frame is set as $x \parallel$ roll direction (RD), $y \parallel$ transverse direction (TD) and $z \parallel$ ND; therefore, the diagonal component e_{33} of the transformed DGT is the key consideration. By transforming the DGTs of the active $\{11\bar{2}2\}$ and $\{10\bar{1}2\}$ twin variants from their respective twin frames into the sample frame, the results turn out that the e_{33} components vary from -0.1 to 0.05 , suggesting that these twins bestow little external strains. Another way to transform from crystal frame into the sample frame is by Euler angle of twin p, which can be obtained by electron backscatter diffraction (EBSD). Schuman et al. [37] adopted this method to calculate the twin formation energy e_{33}/\sqrt{L} , where L is the free path of twin lamella. It is found that in titanium channel die compressed to 16% reduction, active twin variants have the highest absolute value of twin formation energy, not those with the highest SFs.

The twin/detwinning behavior could also be elucidated by transforming DGT from twin or slip frame into the sample frame. Shiyong et al. [35] adopted this method to clarify the twin/detwinning mechanism that $\{10\bar{1}2\}$ twin with negative SF -0.16 appeared at strain 0.1 then disappeared at strain 0.15 inside the same grain. In order to interpret the occurrence of the SF-negative $\{10\bar{1}2\}$ twin, DGTs of the prismatic slip and $\{10\bar{1}2\}$ twin are transformed into the macroscopic sample frame, which is defined as the $x \parallel$ tensile direction, $y \parallel$ transverse direction and $z \parallel$ ND. In such a case, diagonal components of the transformed tensor represent the normal strains in the three principal directions. The results show that prismatic slips at both sides of the grain boundary have positive e_{11} and negative e_{22} and e_{33} , suggesting that strain induced by prismatic slips are in accordance with external strains. As deformation develops, concentrated slip bands pile up at grain boundaries to produce a back stress, which can be released by a twin with locally positive SF but globally negative SF. This has been demonstrated by the negative e_{11} and positive e_{22} and e_{33} of twin shear DGT expressed in the sample frame. As further strain to 0.15, the strong tensile load forces twin to produce a strain state was consistent with the external strain, leading to detwinning.

3.2. DGA between Primary Twin and Neighboring Grain

Accommodation strains that deformation twins imposed on neighboring grains can be evaluated by transform twin DGT from twin frame into the crystal frame of neighboring grains in terms of procedure II in Figure 2. In this routine, DGT of primary twin p is

presented as $e_{ij}^{T^{A \rightarrow p}}$ and transformed into a crystal frame of neighboring grain B expressed as $e_{ij}^{C^B}$. Since the six shear components of DGT in crystal frame have specific physical interpretations, the highest shear components in $e_{ij}^{C^B}$ reveal the most required deformation modes in neighboring grain B that largely accommodate the twin shear from twin p . On the contrary, the lowest shear components reflect the least likely occur deformation modes in neighboring grain.

For deformation twins in Mg and its alloys analyzed with procedure II in Figure 2, a requirement of the prismatic slip in the neighboring grain is the main impedance for twin activation. According to CRSS of Mg, basal slip with the lowest CRSS around 18 MPa is the easiest to activate, followed by $\{10\bar{1}2\}$ twin with CRSS about 23.5 MPa [5], prismatic slip and pyramidal slip or $\{10\bar{1}1\}$ twin. An approximation ratio of CRSS among the four deformation modes is 1:4:9:10 [27]. Although the absolute values of CRSS for individual deformation modes are divergence, the relative order of magnitude is consistent [4–6]. Based on the CRSS order, the twin that demands prismatic slip or pyramidal slip in the neighboring grain is hard to be accommodated, hence it fails to operate even with the high SF. In the extruded AM30 and AZ31 tubes extended along the extrusion direction (ED), Jonas et al. [32] reported that the selected primary twin variants with low SFs (0.05–0.22) require very small accommodation by e_{xy} with an average value below 0.005, while the absent variants with relatively higher SFs (0.4–0.5) indicate larger average e_{xy} that fell in the range 0.025–0.075. Mu et al. [27] also applied this procedure to interpret the variant selection of multigeneration twinning in the AZ31B alloy deformed by channel die compression. During their calculations, primary and secondary twins are considered as the matrix of secondary and tertiary twins, respectively. The neighboring grains of the secondary twins are those that not only surround its matrix but also adjoin tertiary twins. The neighboring grain of tertiary twin is primary twin. Their results also demonstrate that prismatic slip, represented by e_{xy} and/or e_{yx} components is one of the determinant factors in variant selection in Mg. The twin that requires little strain accommodation by a prismatic slip in neighboring grain will operate or grow to a relatively large size; conversely, those that require a large strain by prismatic slip will inactive or exhibit small size.

For deformation twins in Ti employed operation II in Figure 2, variants that could be accommodated by prismatic and/or basal slips in neighboring grains that have a high probability to activate. Conversely, variants that have relatively high SFs but need a pyramidal slip or further twinning in neighboring grains hardly occur, since prismatic slip has the lowest CRSS of 181 MPa amid the deformation modes in Ti, followed by basal slip with CRSS 209 MPa and pyramidal slips or twinning with CRSS around 474 MPa [3]. The absolute CRSS values for each deformation modes usually vary greatly due to the discrepancy in measurements [2,3,38–40], but the relative order is the same. Qin et al. [41] investigated variant selections for the primary twin in pure Ti and evidenced that variants with low SFs (less than 0.2) present as a result of ease accommodation by a prismatic slip in neighboring grain. While variants with potential high SF (larger than 0.4) absent because of its requirement of deformation modes with relatively high CRSSs such as basal, pyramidal slips or twinning. Since the ratios of absent high SF variants to all potential high SF variants for primary, secondary and tertiary twins are 43%, 48% and 80%, respectively, Qin et al. [42] also utilized procedure II in Figure 2 to clear the appearance of low-SF variants and disappearance of high-SF variants in the multigeneration of twinning. Similarly, the primary and secondary twins are taken as the matrix of secondary and tertiary twins, respectively. Regions that connected with their matrix are considered as neighboring grains. The results show that the second and third generation of observed twins are those with low SF but could be easily accommodated by prismatic or basal slips of neighboring grain. However, those with the highest SFs but require “difficult” deformation mode such as absent pyramidal slip.

3.3. DGA between Twin Pairs Across Grain Boundary

Twin–twin and twin–slip pairs across grain boundaries are determined by the capability of strain accommodation which can be characterized by the procedure of case III in Figure 2. During the calculations, DGT in one side twin/slip frame is transformed into the opposite twin/slip frame of the grain boundary. Hence, the e_{13} component of transformed tensor embodies the feasibility of twin/slip accommodated through twin or slip at facing side of the grain boundary. This procedure is also called modified DGA (m-DGA) [36].

DGA analyses based on case III have shed light on the twin–twin and twin–slip pairs generated at both sides of grain boundaries in Ti. Xu et al. [36] used this criterion to explain the $\{11\bar{2}2\}$ – $\{10\bar{1}2\}$ twin pairs presented at both sides of large-angle grain boundaries in compressed Ti. As $\{11\bar{2}2\}$ twins have a much larger size than $\{10\bar{1}2\}$ twins, it is reasonable to consider that the latter twins are stimulated by the former twins. By transforming DGT from the $\{10\bar{1}2\}$ twin frame into that of the $\{11\bar{2}2\}$ frame, it turns out that the stimulated the $\{10\bar{1}2\}$ twin variants are those that can maximumly accommodate the strain induced by active $\{11\bar{2}2\}$ twins rather than those that possess the highest resolved stress or contribute most to external strain. Wang et al. [35] investigated twin–twin pair and twin–slip pair across grain boundaries in extended Ti. Their results turned out that, as the strain increased, the $\{10\bar{1}2\}$ twin in a grain stimulated the $\{11\bar{2}2\}$ twin in neighbor grain, which further aroused the $\{11\bar{2}2\}$ and $\{11\bar{2}4\}$ twins inside another adjacent grain. Similarly, the $\{11\bar{2}2\}$ twin in one grain is often connected to the first order pyramidal slip in its neighbor grain. By transforming DGT of the active twins from their twin frames into potential twin or slip frames of those passively activated deformation modes in neighboring grain, it reveals that all the simulated deformation modes in adjoining grain are those possessing the highest e_{13} values.

By applying the procedure of case III to low-SF $\{10\bar{1}2\}$ twins activated at the grain boundaries in AZ31 alloy, Zhang-Zhi et al. [26] unfolded that strain accommodation capacity of deformation modes in neighboring grain govern activation of those $\{10\bar{1}2\}$ twins. The DGTs of six potential $\{10\bar{1}2\}$ twins at one side of grain boundary are transformed from their respective twin frames into frames of five possible deformation modes in neighboring grain, including slip reference frames of basal, prismatic and pyramidal slips and twin reference frames of the $\{10\bar{1}2\}$ and $\{10\bar{1}1\}$ twins. Since both basal and prismatic slip systems contain three equivalent variants, and the pyramidal slip and twin each has six variants, there are 24 possible variants in neighboring grain in total. Accordingly, six $\{10\bar{1}2\}$ twin variants at one side of the grain boundary can produce 144 possible variants on the other side. For ease to link the e_{13} components to the activation tendency, two variables γ^i and ε^i are introduced. γ^i is defined as the maximum e_{13} of accommodation mode i divided by the maximum e_{13} among the six $\{10\bar{1}2\}$ variants. ε^i is defined as the minimum e_{13} component of the accommodation mode i among the six $\{10\bar{1}2\}$ variants divided by e_{13} of each variant. With such a definition, the most probable accommodation mode presents a higher γ^i value and the lower ε^i value. The results show that $\{10\bar{1}2\}$ twins activated only at one side of the boundary require accommodation by the most easily activated basal slip in a neighboring grain, while the $\{10\bar{1}2\}$ twin pair across a boundary requires a more prismatic slip and/or $\{10\bar{1}2\}$ twinning but less pyramidal slip and/or $\{10\bar{1}1\}$ twin in neighboring grain.

In addition to the DGA evaluation, another criterion applied in interpreting twin–twin pair, twin–slip pair or slip–slip pair across a grain boundary is geometric compatibility factor m' , which is defined as $\cos\kappa \cdot \cos\Phi$ by Lusters and Morris [43]. Here, κ is the angle between slip/twin directions, and Φ is the angle between slip/twin plane. The geometric compatibility factor also successfully explained behaviors of twin pairs across grain boundary and slip transmit grain boundary in both Ti and Mg [26,33,44–47].

3.4. DGA between Primary Twin Variants with the Same Grain

Twin variants of different modes activated in the same parent and contact with each other are probably those that can easily accommodate each other and, therefore, can be elucidated using procedure IV in Figure 2. Xu et al. [9] reported a typical example of such a

case that the primary $\{10\bar{1}2\}$ twin variant denoted as T_2^I occurred at the obtuse angle area of primary $\{11\bar{2}1\}$ twin. Local stress analysis and SF calculations predict the location and $\{10\bar{1}2\}$ twin series but fail to clear the active variant with the second higher SFs. By transforming twin shear tensor of the operating primary $\{11\bar{2}1\}$ twins into the twin frame of six potential $\{10\bar{1}2\}$ twin variants and into the other four potential $\{11\bar{2}1\}$ twin variants, it clearly shows that the variant T_2^I has the largest e_{13} value that could maximumly accommodate the strains resulted from the $\{11\bar{2}1\}$ twin. Another case is the primary $\{10\bar{1}2\}$ variants represented by T_3^I and T_4^I developed in the parent grain, along with the $\{11\bar{2}1\}$ twin variants T_3^{II} in Ti shocked by a split Hopkinson pressure bar at strain rate $\sim 10^3 \text{ s}^{-1}$ [48]. Twin shear tensor of the active primary $\{11\bar{2}1\}$ twin is transferred to the twin frame of the six potential $\{10\bar{1}2\}$ twin variants in the same parent. The result reveals that the operative $\{10\bar{1}2\}$ twin variants exhibit the highest e_{13} components.

3.5. DGA between Primary and Second Twins

Four different ways of evaluating strain accommodation of second-generation twinning in Ti and Mg have been conducted. Firstly, Ando et al. [30] proposed a method to examine the strain accommodations induced by $\{10\bar{1}1\}$ - $\{10\bar{1}2\}$ double twins in AZ31 alloy. In their operations, twinning shear tensors of the primary $\{10\bar{1}1\}$ and secondary $\{10\bar{1}2\}$ twins are transformed from their respective twin frames into the crystal frame of the parent grain named as a standard coordinate system. For the secondary twin, twinning shear tensor in its twin frame is firstly transformed into crystal frame of primary twin, then further transformed into crystal frame of parent grain. The transformation matrices are derived in terms of the angle-axis pairs between twinning and their matrices. The total accommodation of the $\{10\bar{1}1\}$ - $\{10\bar{1}2\}$ double twin is obtained by adding the strain tensor induced by the primary twin and secondary twin. With this calculation, it suggests that the $\{10\bar{1}1\}$ - $\{10\bar{1}2\}$ double twin with the same planes of shear between the primary and second twins are more active compared to the $\{10\bar{1}1\}$ - $\{10\bar{1}2\}$ double twin with a different plane of shear, because the former induces are much smaller strains in the parent grain. This method considers the overall strain of the transformed tensor instead of a specific component. However, Martin et al. [31] found that, in their investigation of $\{10\bar{1}1\}$ - $\{10\bar{1}2\}$ double twin in extended AM30, the total accommodation of strains produced by primary and secondary twins inside the parent grain cannot discriminate the prevalent twin group. Secondly, Qin et al. [42] adopted procedure II in Figure 2 to investigate strain accommodation for $\{10\bar{1}2\}$ - $\{11\bar{2}2\}$ and $\{11\bar{2}2\}$ - $\{10\bar{1}2\}$ double twins in pure Ti compressed to a large strain of 30%. It should be very cautious to select the appropriate neighboring grains for secondary twins when using this method. However, this way of evaluation seems to be not very effective in explaining the prevalence of some kinds of secondary twins observed in Ti at relatively low strain around 9% [21]. Thirdly, Xu et al. [9] tried to account for strain accommodation of the $\{11\bar{2}2\}$ - $\{10\bar{1}2\}$ double twins in Ti by transforming DGT of the primary twin from its twin reference frame into the twin frame of the secondary twin. Still, this way cannot distinguish the popularity of specific variants of the secondary twins, especially for that of the rare occurred multiple twinning. Finally, a method that transforms the DGA of the secondary twin into the primary twin frame brings insights into the selection of the secondary twin variants. This is the procedure V shown in Figure 2, which will be discussed in the following.

Generally, variants that can maximumly accommodate the twin shear results from primary twins that would tend to activate. This accommodation ability can be described by evaluating the resultant e_{13} components obtained by procedure V. As to Ti, five types of secondary twins have been successfully predicted, adopting this method, including co-family double twinning of $\{11\bar{2}2\}$ - $\{11\bar{2}1\}$, $\{11\bar{2}1\}$ - $\{11\bar{2}4\}$, $\{11\bar{2}1\}$ - $\{11\bar{2}2\}$ and non-family double twinning of $\{11\bar{2}2\}$ - $\{10\bar{1}2\}$ and $\{11\bar{2}4\}$ - $\{10\bar{1}2\}$ [11,21,48]. The results showed that all the active secondary twin variants possess the highest e_{13} components that transformed into the twin frame of the primary twins, suggesting that the selected secondary twin variants could maximum diminish twin shear strain induced by corresponding primary twins.

A phenomenon worthy to note is that secondary $\{10\bar{1}2\}$ twinning inside primary $\{11\bar{2}4\}$ twins usually accompany by co-zone the $\{11\bar{2}2\}$ twin [21,48]. The secondary $\{10\bar{1}2\}$ twin is demonstrated as the one that can maximally accommodate strain from the primary twin by transforming the deformation gradient of the $\{10\bar{1}2\}$ twin from its twin frame into the primary twin frame. While the secondary $\{10\bar{1}2\}$ twin variants T_3^I and T_4^I stimulated inside the $\{11\bar{2}4\}$ twin variant C_6^{II} was ascribed to accommodate the twinning shear induced by the incoming $\{11\bar{2}2\}$ twin variant C_3^I , since both the active secondary twin variants have the highest e_{13} component transformed from the operative $\{11\bar{2}2\}$ twin into the twin frames of the six potential $\{10\bar{1}2\}$ twin variants. Interestingly, Martin et al. [31] did not adopt this approach to explain the active secondary twin group in AM30 alloy, but their calculation results demonstrated that the two operative groups exhibit a higher e_{13} compared to those absent.

4. Summary

The discourse gives a brief narrative over strain accommodations among twin variants in the Ti and Mg alloys. The strain accommodation is one of the key factors affecting twin variant selections during plastic deformation and can be quantitatively evaluated by the transformation of displacement gradient tensor of twinning shear. These strain accommodations are classified into five categories in terms of different regions where the primary twin imposes influence. These regions include sample entirety, neighboring grain, adjoining twin in neighboring grain, other primary twin variants adjacent to the primary twin inside the same parent grain and secondary generation twins inside the primary twin. By investigating the potentially required deformation modes that need to accommodate strains resulted from twinning, it reveals that twin variants have easily been accommodated by its vicinity are more prone to operate, conversely, those withstanding relatively high resolved shear stress but hard to be accommodated are absent. The displacement gradient accommodation criterion gains success in the interpretation of the non-Schmid behavior and provides a necessary supplement in the twin variant selection rules.

Generally, Schmid factors and accommodation strains could be integrated as deformation energy taking account of both the stress and strain [49]. Deformation modes that would maximumly exhaust an external work are expected to happen, such as deformation modes across grain boundaries such as twin–twin, slip–slip and twin–twin pairs; another usually adopted criterion is the geometric compatibility factor, which reflects the strain compatibility between deformation modes at both sides of the grain boundary by resolving the strain induced by one side deformation onto that of at the opposite side of the grain boundary.

Funding: This research was funded by National Natural Science Foundation of China Youth Fund, grant number 52001287.

Institutional Review Board Statement: Not applicable.

Informed Consent Statement: Not applicable.

Data Availability Statement: Data sharing not applicable.

Acknowledgments: The authors thank Shun Xu for useful discussion in the DGT calculations.

Conflicts of Interest: The authors declare no conflict of interest.

Appendix A.

Appendix A.1. Transformation from Twin Frame $T^{A \rightarrow p}$ into Sample Frame S

Suppose r is the c/a ratio of hcp-structured metals, and s is the twinning shear of a specific twin; then, the displacement gradient tensor (DGA) of primary twin p in twin frame $T^{A \rightarrow p}$ can be expressed as:

$$e_{ij}^{T^{A \rightarrow p}} = \begin{pmatrix} 0 & 0 & s \\ 0 & 0 & 0 \\ 0 & 0 & 0 \end{pmatrix}$$

In frame $T^{A \rightarrow p}$, the x^{Ap} and z^{Ap} axes are set parallel to the twinning shear direction $[uvtw]$ and normal of the twinning plane $(hkil)$ of primary twin p , respectively. Note that Miller-Bravais indices $(hkil)[uvtw]$ for primary twin p are expressed in the hcp lattice of parent grain A ; therefore, they need to be transformed into orthogonal coordinate system by the following relations:

$$\begin{cases} x'_1 = \sqrt{3}(u + v/2) \\ x'_2 = 3v/2 \\ x'_3 = wr \end{cases} \quad \begin{cases} z'_1 = (2h + k) \\ z'_2 = \sqrt{3}k \\ z'_3 = \sqrt{3}l/r \end{cases}$$

Normalize axes x^{Ap} and z^{Ap} as unit lengths by dividing their respective mode:

$$|x^{Ap}| = \sqrt{3(u + v/2)^2 + 9v^2/4 + w^2r^2}, \quad |z^{Ap}| = \sqrt{(2h + k)^2 + 3k^2 + 3l^2/r^2}$$

The y -axis is determined by a cross-product of $z^{Ap} \otimes x^{Ap}$; then, the base vectors of the orthogonal coordinate systems $\{x^{Ap}, y^{Ap}, z^{Ap}\}$ can be expressed as below:

$$\begin{cases} x_1^{Ap} = [\sqrt{3}(u + v/2)]/|x^{Ap}| \\ x_2^{Ap} = 3v/(2|x^{Ap}|) \\ x_3^{Ap} = wr/|x^{Ap}| \end{cases} \quad \begin{cases} z_1^{Ap} = (2h + k)/|z^{Ap}| \\ z_2^{Ap} = \sqrt{3}k/|z^{Ap}| \\ z_3^{Ap} = \sqrt{3}l/(r|z^{Ap}|) \end{cases} \quad \begin{cases} y_1^{Ap} = x_3^{Ap}z_2^{Ap} - x_2^{Ap}z_3^{Ap} \\ y_2^{Ap} = x_1^{Ap}z_3^{Ap} - x_3^{Ap}z_1^{Ap} \\ y_3^{Ap} = x_2^{Ap}z_1^{Ap} - x_1^{Ap}z_2^{Ap} \end{cases} \quad (A1)$$

Hence, the transformation matrix $h_{A \rightarrow p}$ is obtained as:

$$h_{A \rightarrow p} = (x^{Ap} \quad y^{Ap} \quad z^{Ap}) = \begin{pmatrix} x_1^{Ap} & y_1^{Ap} & z_1^{Ap} \\ x_2^{Ap} & y_2^{Ap} & z_2^{Ap} \\ x_3^{Ap} & y_3^{Ap} & z_3^{Ap} \end{pmatrix} \quad (A2)$$

The $h_{A \rightarrow p}$ transforms $e_{ij}^{T^{A \rightarrow p}}$ from twin frame $T^{A \rightarrow p}$ into crystal frame C^A according to equation $e_{ij}^{C^A} = h_{A \rightarrow p} * e_{ij}^{T^{A \rightarrow p}} * h_{A \rightarrow p}^{-1}$.

Since the Euler angle of the parent grain A of $(\varphi_1^A \quad \Phi^A \quad \varphi_2^A)$ represents the rotation of sample frame in order to coincide with the crystal frame of a grain, the rotation matrix g_A of parent grain A could be depicted as [50]:

$$g_A = \begin{pmatrix} \cos\varphi_2^A & \sin\varphi_2^A & 0 \\ -\sin\varphi_2^A & \cos\varphi_2^A & 0 \\ 0 & 0 & 1 \end{pmatrix} \begin{pmatrix} 1 & 0 & 0 \\ 0 & \cos\Phi^A & \sin\Phi^A \\ 0 & -\sin\Phi^A & \cos\Phi^A \end{pmatrix} \begin{pmatrix} \cos\varphi_1^A & \sin\varphi_1^A & 0 \\ -\sin\varphi_1^A & \cos\varphi_1^A & 0 \\ 0 & 0 & 1 \end{pmatrix} \quad (A3)$$

Therefore, $e_{ij}^{C^A}$ can be further transformed into a sample frame as e_{ij}^S in terms of relation:

$$e_{ij}^S = g_A^{-1} * e_{ij}^{C^A} * g_A = g_A^{-1} * h_{A \rightarrow p} * e_{ij}^{T^{A \rightarrow p}} * h_{A \rightarrow p}^{-1} * g_A \quad (A4)$$

If the Euler angle of primary twin p is known as $(\varphi_1^p \ \Phi^p \ \varphi_2^p)$, then the DGT of primary twin p can be directly transformed into sample frame by relation:

$$e_{ij}^S = g_p^{-1} * e_{ij}^{T^{A \rightarrow p}} * g_p \quad (A5)$$

Appendix A.2. Transformation from Twin Frame $T^{A \rightarrow p}$ of Primary Twin p in Parent Grain A into Crystal Frame C^B of Neighboring Grain B

Assume the Euler angle of neighboring grain B is presented as $(\varphi_1^B \ \Phi^B \ \varphi_2^B)$, the DGT of primary twin p could be further transformed into the crystal frame of neighboring grain B based on Equation (A4) with rotation matrix g_B as following:

$$e_{ij}^{C^B} = g_B * e_{ij}^S * g_B^{-1} = g_B * g_A^{-1} * h_{A \rightarrow p} * e_{ij}^{T^{A \rightarrow p}} * h_{A \rightarrow p}^{-1} * g_A * g_B^{-1} \quad (A6)$$

Appendix A.3. Transformation from Twin Frame $T^{A \rightarrow p}$ of Primary Twin p inside Parent Grain A into Twin Frame $T^{B \rightarrow n}$ of Primary Twin n in Neighboring Grain B

The twin frame $T^{B \rightarrow n}$ of the primary twin n in neighboring grain B is defined in the same way as described by Equation (A1). As a result, the base vectors $\{x^n, y^n, z^n\}$ of twin frame $T^{B \rightarrow n}$ constitute the transformation matrix $h_{B \rightarrow n}$:

$$h_{B \rightarrow n} = (x^n \ y^n \ z^n) = \begin{pmatrix} x_1^n & y_1^n & z_1^n \\ x_2^n & y_2^n & z_2^n \\ x_3^n & y_3^n & z_3^n \end{pmatrix}$$

Therefore, the DGT of primary twin p in grain A can be transformed into twin frame n in grain B based on Equation (A6) as following:

$$e_{ij}^{T^{B \rightarrow n}} = h_{B \rightarrow n} * e_{ij}^{C^B} * h_{B \rightarrow n}^{-1} = h_{B \rightarrow n} * g_B * g_A^{-1} * h_{A \rightarrow p} * e_{ij}^{T^{A \rightarrow p}} * h_{A \rightarrow p}^{-1} * g_A * g_B^{-1} * h_{B \rightarrow n}^{-1} \quad (A7)$$

Appendix A.4. Transformation from Twin Frame $T^{A \rightarrow p}$ of Primary Twin p into Twin Frame $T^{A \rightarrow v}$ of Primary Twin v within the Same Parent Grain A

This transformation is related to transformation matrices $h_{A \rightarrow p}$ and $h_{A \rightarrow v}$, both of which are determined by the same approach as Equations (A1) and (A2). Here, the matrix $h_{A \rightarrow v}$ is determined by twinning indices of primary twin v in parent grain A. Thus, the transformation from $e_{ij}^{T^{A \rightarrow p}}$ into $e_{ij}^{T^{A \rightarrow v}}$ is expressed as:

$$e_{ij}^{T^{A \rightarrow v}} = h_{A \rightarrow v}^{-1} * h_{A \rightarrow p} * e_{ij}^{T^{A \rightarrow p}} * h_{A \rightarrow p}^{-1} * h_{A \rightarrow v}$$

Appendix A.5. Transformation from Twin Frame $T^{p \rightarrow s}$ of Secondary Twin s Expressed in Primary Twin p into Twin Frame T^p of Primary Twin p

To derive the DGT transformation expression between secondary twin s and primary twin p , transformation matrices related to procedure V in Figure 2 should be established at first.

Matrix h_1 can transform the twin frame $T^{A \rightarrow p}$ of primary twin p into twin frame T^p . If the primary twin p is type I twinning with rational indices of K_1 and η_2 that satisfy the symmetry of rotating 180° around K_1 normal, then h_1 is expressed as:

$$h_1 = \begin{pmatrix} -1 & 0 & 0 \\ 0 & -1 & 0 \\ 0 & 0 & 1 \end{pmatrix}$$

If p is a type II twinning with symmetry of rotating 180° around η_1 , then h_1 gets expressed as:

$$h_1 = \begin{pmatrix} 1 & 0 & 0 \\ 0 & -1 & 0 \\ 0 & 0 & -1 \end{pmatrix}$$

Matrix h_p rotates the twin frame T^p of primary twin p into crystal frame C^p of the primary twin p . Therefore, h_p is determined by the twin parameters of primary twin p expressed inside the twinned crystal and can be obtained according to the same way in Equations (A1) and (A2). Taking the base vectors of frame T^p as $\{x^p, y^p, z^p\}$, the transformation matrix h_p is expressed as follow:

$$h_p = (x^p, y^p, z^p) = \begin{pmatrix} x_1^p & y_1^p & z_1^p \\ x_2^p & y_2^p & z_2^p \\ x_3^p & y_3^p & z_3^p \end{pmatrix}$$

Matrix $h_{p \rightarrow s}$ rotates crystal frame C^p of primary twin p into twin frame $T^{p \rightarrow s}$ of secondary twin s , which is expressed inside the primary twin lattice. As the same approach determining the h_p matrix, $h_{p \rightarrow s}$ is fixed by twin parameters of the secondary twin expressed in the lattice of primary twin p using Equations (A1) and (A2). Taking the base vectors of twin frame $T^{p \rightarrow s}$ as $\{x^s, y^s, z^s\}$, the $h_{p \rightarrow s}$ is expressed as follows:

$$h_{p \rightarrow s} = (x^s, y^s, z^s) = \begin{pmatrix} x_1^s & y_1^s & z_1^s \\ x_2^s & y_2^s & z_2^s \\ x_3^s & y_3^s & z_3^s \end{pmatrix}$$

Finally, the $e_{ij}^{T^{p \rightarrow s}}$ in the secondary twin frame can be transformed into the primary twin frame expressed as $e_{ij}^{T^p}$, according to the following equation:

$$e_{ij}^{T^p} = h_p^{-1} * h_{p \rightarrow s} * e_{ij}^{T^{p \rightarrow s}} * h_{p \rightarrow s}^{-1} * h_p$$

References

- Schmid, E.; Boas, W. *Plasticity of Crystals with Special Reference to Metal*; F.A. Hughes: London, UK, 1950.
- Wu, X.; Kalidindi, S.R.; Necker, C.; Salem, A.A. Prediction of crystallographic texture evolution and anisotropic stress-strain curves during large plastic strains in high purity α -titanium using a Taylor-type crystal plasticity model. *Acta Mater.* **2007**, *55*, 423–432. [[CrossRef](#)]
- Gong, J.; Wilkinson, A.J. Anisotropy in the plastic flow properties of single-crystal α titanium determined from micro-cantilever beams. *Acta Mater.* **2009**, *57*, 5693–5705. [[CrossRef](#)]
- Yu, Q.; Zhang, J.; Jiang, Y. Direct observation of twinning–detwinning–retwinning on magnesium single crystal subjected to strain-controlled cyclic tension–compression in $[0\ 0\ 0\ 1]$ direction. *Philos. Mag. Lett.* **2011**, *91*, 757–765. [[CrossRef](#)]
- Lynch, P.A.; Kunz, M.; Tamura, N.; Barnett, M.R. Time and spatial resolution of slip and twinning in a grain embedded within a magnesium polycrystal. *Acta Mater.* **2014**, *78*, 203–212. [[CrossRef](#)]
- Liu, Y.; Li, N.; Arul Kumar, M.; Pathak, S.; Wang, J.; McCabe, R.J.; Mara, N.A.; Tomé, C.N. Experimentally quantifying critical stresses associated with basal slip and twinning in magnesium using micropillars. *Acta Mater.* **2017**, *135*, 411–421. [[CrossRef](#)]
- Nan, X.-L.; Wang, H.-Y.; Zhang, L.; Li, J.-B.; Jiang, Q.-C. Calculation of Schmid factors in magnesium: Analysis of deformation behaviors. *Scr. Mater.* **2012**, *67*, 443–446. [[CrossRef](#)]
- Yu, Q.; Wang, J.; Jiang, Y.; McCabe, R.J.; Li, N.; Tomé, C.N. Twin–twin interactions in magnesium. *Acta Mater.* **2014**, *77*, 28–42. [[CrossRef](#)]
- Xu, S.; Gong, M.; Schuman, C.; Lecomte, J.-S.; Xie, X.; Wang, J. Sequential $\{10\text{--}12\}$ twinning stimulated by other twins in titanium. *Acta Mater.* **2017**, *132*, 57–68. [[CrossRef](#)]
- Xu, S.; Gong, M.; Xie, X.; Liu, Y.; Schuman, C.; Lecomte, J.-S.; Wang, J. Crystallographic characters of $\{11\text{--}22\}$ twin–twin junctions in titanium. *Philos. Mag. Lett.* **2017**, *97*, 429–441. [[CrossRef](#)]
- Zhou, P.; Xu, S.; Xiao, D.; Jiang, C.; Hu, Y.; Wang, J. Shock-induced $\{11\text{--}21\} \rightarrow \{11\text{--}22\}$ double twinning in titanium. *Int. J. Plast.* **2019**, *112*, 194–205. [[CrossRef](#)]
- Bao, L.; Schuman, C.; Le, Q.c.; Lecomte, J.S.; Zhang, Z.; Philippe, M.-J.; Cui, J.; Esling, C. A novel method for predicting variant selection during primary, secondary and tertiary twinning in titanium. *Mater. Lett.* **2014**, *132*, 162–166. [[CrossRef](#)]

13. Shi, D.; Liu, T.; Hou, D.; Chen, H.; Pan, F.; Chen, H. The effect of twin–twin interaction in Mg₃Al₁Zn alloy during compression. *J. Alloys Compd.* **2016**, *685*, 428–435. [[CrossRef](#)]
14. Deng, X.G.; Hui, S.X.; Ye, W.J.; Song, X.Y. Analysis of twinning behavior of pure Ti compressed at different strain rates by Schmid factor. *Mater. Sci. Eng. A* **2013**, *575*, 15–20.
15. Yu, Q.; Jiang, Y.; Wang, J. Tension-compression-tension tertiary twins in coarse-grained polycrystalline pure magnesium at room temperature. *Philos. Mag. Lett.* **2015**, *95*, 194–201. [[CrossRef](#)]
16. Yu, Q.; Jiang, Y.; Wang, J. Cyclic deformation and fatigue damage in single-crystal magnesium under fully reversed strain-controlled tension-compression in the [1010] direction. *Scr. Mater.* **2015**, *96*, 41–44. [[CrossRef](#)]
17. Qiao, H.; Barnett, M.R.; Wu, P.D. Modeling of twin formation, propagation and growth in a Mg single crystal based on crystal plasticity finite element method. *Int. J. Plast.* **2016**, *86*. [[CrossRef](#)]
18. Chen, H.; Liu, T.; Hou, D.; Shi, D. Study on the paired twinning behavior in a hot rolled AZ31 magnesium alloy via interrupted in situ compression. *Mater. Sci. Eng. A* **2016**, *667*, 402–408. [[CrossRef](#)]
19. Godet, S.; Jiang, L.; Luo, A.A.; Jonas, J.J. Use of Schmid factors to select extension twin variants in extruded magnesium alloy tubes. *Scr. Mater.* **2006**, *55*, 1055–1058. [[CrossRef](#)]
20. Lainé, S.J.; Knowles, K.M. {11–24} deformation twinning in commercial purity titanium at room temperature. *Philos. Mag.* **2015**, *95*, 2153–2166. [[CrossRef](#)]
21. Xu, S.; Gong, M.; Jiang, Y.; Schuman, C.; Lecomte, J.-S.; Wang, J. Secondary twin variant selection in four types of double twins in titanium. *Acta Mater.* **2018**, *152*, 58–76. [[CrossRef](#)]
22. Li, X.; Li, J.; Zhou, B.; Yu, M.; Sui, M. Interaction of {11–22} twin variants in hexagonal close-packed titanium. *J. Mater. Sci. Technol.* **2019**, *35*, 660–666. [[CrossRef](#)]
23. Barnett, M.R.; Keshavarz, Z.; Beer, A.G.; Ma, X. Non-Schmid behaviour during secondary twinning in a polycrystalline magnesium alloy. *Acta Mater.* **2008**, *56*, 5–15. [[CrossRef](#)]
24. Barrett, C.D.; El Kadiri, H.; Tschopp, M.A. Breakdown of the Schmid law in homogeneous and heterogeneous nucleation events of slip and twinning in magnesium. *J. Mech. Phys. Solids* **2012**, *60*, 2084–2099. [[CrossRef](#)]
25. Shi, Z.-Z.; Zhang, Y.; Wagner, F.; Richeton, T.; Juan, P.-A.; Lecomte, J.-S.; Capolungo, L.; Berbenni, S. Sequential double extension twinning in a magnesium alloy: Combined statistical and micromechanical analyses. *Acta Mater.* **2015**, *96*, 333–343. [[CrossRef](#)]
26. Shi, Z.-Z.; Zhang, Y.; Wagner, F.; Juan, P.-A.; Berbenni, S.; Capolungo, L.; Lecomte, J.-S.; Richeton, T. On the selection of extension twin variants with low Schmid factors in a deformed Mg alloy. *Acta Mater.* **2015**, *83*, 17–28. [[CrossRef](#)]
27. Mu, S.; Jonas, J.J.; Gottstein, G. Variant selection of primary, secondary and tertiary twins in a deformed Mg alloy. *Acta Mater.* **2012**, *60*, 2043–2053. [[CrossRef](#)]
28. Zhu, B.; Liu, X.; Xie, C.; Wu, Y.; Zhang, J. {10–12} extension twin variant selection under a high strain rate in AZ31 magnesium alloy during the plane strain compression. *Vacuum* **2019**, *160*, 279–285. [[CrossRef](#)]
29. Mahajan, S.; Chin, G.Y. Twin-slip, twin-twin and slip-twin interactions in Co-8 wt.% Fe alloy single crystals. *Acta Metall.* **1973**, *21*, 173–179. [[CrossRef](#)]
30. Ando, D.; Koike, J.; Sutou, Y. Relationship between deformation twinning and surface step formation in AZ31 magnesium alloys. *Acta Mater.* **2010**, *58*, 4316–4324. [[CrossRef](#)]
31. Martin, E.; Capolungo, L.; Jiang, L.; Jonas, J.J. Variant selection during secondary twinning in Mg-3%Al. *Acta Mater.* **2010**, *58*, 3970–3983. [[CrossRef](#)]
32. Jonas, J.J.; Mu, S.; Al-Samman, T.; Gottstein, G.; Jiang, L.; Martin, E. The role of strain accommodation during the variant selection of primary twins in magnesium. *Acta Mater.* **2011**, *59*, 2046–2056. [[CrossRef](#)]
33. Wang, L.; Yang, Y.; Eisenlohr, P.; Bieler, T.R.; Crimp, M.A.; Mason, D.E. Twin Nucleation by Slip Transfer across Grain Boundaries in Commercial Purity Titanium. *Metall. Mater. Trans. A* **2010**, *41*, 421–430. [[CrossRef](#)]
34. Capolungo, L.; Beyerlein, I.J.; Tome, C.N. Slip-assisted twin growth in hexagonal close-packed metals. *Scr. Mater.* **2009**, *60*, 32–35. [[CrossRef](#)]
35. Wang, S.; Zhang, Y.; Schuman, C.; Lecomte, J.-S. Study of twinning/detwinning behaviors of Ti by interrupted in situ tensile tests. *Acta Mater.* **2015**, *82*, 424–436. [[CrossRef](#)]
36. Xu, S.; Schuman, C.; Lecomte, J.-S. Accommodative $10\bar{1}2$ twins at high angle grain boundaries in rolled pure titanium. *Scr. Mater.* **2016**, *116*, 152–156. [[CrossRef](#)]
37. Schuman, C.; Bao, L.; Lecomte, J.S.b.; Zhang, Y.; Raulot, J.M.; Philippe, M.J.; Esling, C. A new variant selection criterion for twin variants in titanium alloys (Part I). *Adv. Eng. Mater.* **2011**, *13*, 1114–1121. [[CrossRef](#)]
38. Hutchinson, W.B.; Barnett, M.R. Effective values of critical resolved shear stress for slip in polycrystalline magnesium and other hcp metals. *Scr. Mater.* **2010**, *63*, 737–740. [[CrossRef](#)]
39. Poty, A.; Raulot, J.M.; Xu, H.; Bai, J.; Schuman, C.; Lecomte, J.S.; Philippe, M.J.; Esling, C. Classification of the critical resolved shear stress in the hexagonal-close-packed materials by atomic simulation: Application to α -zirconium and α -titanium. *J. Appl. Phys.* **2011**, *110*, 014905. [[CrossRef](#)]
40. Zambaldi, C.; Yang, Y.; Bieler, T.R.; Raabe, D. Orientation informed nanoindentation of α -titanium: Indentation pileup in hexagonal metals deforming by prismatic slip. *J. Mater. Res.* **2011**, *27*, 356–367. [[CrossRef](#)]
41. Qin, H.; Jonas, J.J.; Yu, H.B.; Brodusch, N.; Gauvin, R.; Zhang, X.Y. Initiation and accommodation of primary twins in high-purity titanium. *Acta Mater.* **2014**, *71*, 293–305. [[CrossRef](#)]

42. Qin, H.; Jonas, J.J. Variant selection during secondary and tertiary twinning in pure titanium. *Acta Mater.* **2014**, *75*, 198–211. [[CrossRef](#)]
43. Luster, J.; Morris, M.A. Compatibility of deformation in two-phase Ti-Al alloys: Dependence on microstructure and orientation relationships. *Metall. Mater. Trans. A* **1995**, *26*, 1745–1756. [[CrossRef](#)]
44. Wang, L.; Eisenlohr, P.; Yang, Y.; Bieler, T.R.; Crimp, M.A. Nucleation of paired twins at grain boundaries in titanium. *Scr. Mater.* **2010**, *63*, 827–830. [[CrossRef](#)]
45. Barnett, M.R.; Nave, M.D.; Ghaderi, A. Yield point elongation due to twinning in a magnesium alloy. *Acta Mater.* **2012**, *60*, 1433–1443. [[CrossRef](#)]
46. Xin, R.L.; Guo, C.F.; Xu, Z.R.; Liu, G.D.; Huang, X.X.; Liu, Q. Characteristics of long {10–12} twin bands in sheet rolling of a magnesium alloy. *Scr. Mater.* **2014**, *74*, 96–99. [[CrossRef](#)]
47. Guo, C.; Xin, R.; Ding, C.; Song, B.; Liu, Q. Understanding of variant selection and twin patterns in compressed Mg alloy sheets via combined analysis of Schmid factor and strain compatibility factor. *Mater. Sci. Eng. A* **2014**, *609*, 92–101. [[CrossRef](#)]
48. Xu, S.; Zhou, P.; Liu, G.; Xiao, D.; Gong, M.; Wang, J. Shock-induced two types of {10–12} sequential twinning in Titanium. *Acta Mater.* **2019**, *165*, 547–560. [[CrossRef](#)]
49. Hua, K.; Zhang, Y.; Gan, W.; Kou, H.; Li, J.; Esling, C. Correlation between imposed deformation and transformation lattice strain on α variant selection in a metastable β -Ti alloy under isothermal compression. *Acta Mater.* **2018**, *161*, 150–160. [[CrossRef](#)]
50. Bunge, H.J. *Texture Analysis in Materials Science_Mathematical Methods*; Butterworth: Boston, MA, USA, 1982.